



Spatiotemporal Analysis of Land Cover Changes in Al-Hubail Wetland (Kingdom of Saudi Arabia)

Walid Chouari^{1,2} 

Received: 21 December 2021 / Accepted: 15 December 2022 / Published online: 4 January 2023
© Indian Society of Remote Sensing 2023

Abstract

Land cover dynamics were analyzed temporally and spatially in the Al-Hubail wetland (Al-Ahsa, Kingdom of Saudi Arabia) to determine the evolution of the environmental status of this biologically and ecologically interesting area in Saudi Arabia. Using remote sensing data, land cover changes were estimated for 36 years (1985–2021). For this analysis, three images from 1985 (Landsat 5 MSS), 2003 (Landsat 7 ETM +), and 2021 (Sentinel-2) were used to classify and detect changes. A machine learning algorithm was used, and the images were classified into four main land cover classes: Water bodies, hydromorphic areas, vegetation, and open ground. Change detection was performed for the year pairs 1985 to 2003 and 2003 to 2021. The results of this classification showed a significant increase in the area of hydromorphic areas and vegetation. The results were checked with a confusion matrix indicating an overall accuracy between 89.3 and 92.8%. The qualitative trend data show that the Al-Hubail wetland has changed significantly during the study period. Thus, a significant expansion of the wetland was observed in conjunction with an increase in agricultural drainage toward the wetland. This analysis shows the strong anthropogenic pressure on the area and highlights the need to strengthen the existing laws to preserve local biodiversity in the long term. It suggests that more efforts should be made to manage the water resources of the region effectively.

Keywords Land cover · Classification · Change detection · Al-Hubail wetland

Introduction

Despite their multiple functions and services to human society, wetlands are among the most threatened ecosystems worldwide by human activities: Pollution, use of biological resources, alteration of natural systems, impacts of agricultural activities, etc. (Gardner & Finlayson, 2018; Van Asselen et al., 2013; Xu et al., 2019). The Al-Ahsa region in Saudi Arabia is characterized by a great diversity of wetland ecosystems and natural resources. This diversity is related to the large number of endemic species they host (Al-Dakheel et al., 2009; Al-Hussaini, 2005; Al-Sheikh & Fathi, 2010; Chouari, 2021b; Eid et al., 2020; Fathi et al., 2009; Salih, 2018; Youssef et al., 2009). However,

establishing a drainage network in Al-Ahsa Oasis has led to increasing pressures on natural ecosystems and their biodiversity. These human pressures, depending on their intensity, lead to quantitative (degradation or fluctuation of the ecosystems' surface) and/or qualitative changes, resulting in dysfunction and loss of bioecological values of the natural environments (Abdel-Moneim, 2014; Almadini & Hassaballa, 2019; Al-Obaid et al., 2017; Chouari, 2021b).

This paper aims to analyze the land cover evolution in the Al-Hubail wetland through a mapping method using multidata satellite imagery and a geographic information system (GIS). Remote sensing is a powerful tool for studying environmental issues (Al-Hussaini, 2005; Almadini & Hassaballa, 2019; Chouari, 2021a, 2021b; Maimaitijiang et al., 2015; Petropoulos et al., 2015; Rapinel et al., 2015). Satellite imagery provides valuable large-scale and multi-temporal data on land cover change.

Image segmentation (texture line detection) is a key problem in image processing. The classification is a

✉ Walid Chouari
wchouari@kfu.edu.sa; walidchouari@yahoo.fr

¹ Department of Geography, College of Arts, King Faisal University, Al-Ahsa, Saudi Arabia

² SYFACTE Laboratory, University of Sfax, Sfax, Tunisia

significant step in this process. Classification seeks to extract as much information as possible from images to portray them in a comprehensible and interpretable manner. An array of change detection methods works by calculating a statistical probability of change. Post-classification comparisons (PCCs) are commonly used (Coppin et al., 2004; Deng et al., 2008; Lu et al., 2004; Wu et al., 2017). Post-classification comparisons examine changes between independently classified land cover data over time. The simplest approach to detecting changes is the post-classification comparison technique (PCC). PCCs techniques are based on correctly coding the classification findings for times 1 and 2 and correlating separately produced classed images (Singh, 1989). Post-classification classifications look at how land cover data have changed over time after being classed independently. The output is a change map that shows the entire change matrix. Post-classification comparisons have the following advantages: (1) They eliminate the purpose for precise radiometric calibration and reduce the effect of the atmospheric, sensor, and environmental differences between multi-temporal images; and (2) the technique provide a comprehensive matrix of change directions in comparison to image differentiation. However, Macleod and Congalton (1998) report that post-classification comparisons have significant limitations since they incorporate the inaccuracies of both classifications. The PCC method is hampered by map creation issues and is susceptible to cumulative errors (Chen et al., 2003). A significant amount of auxiliary data must also be given to classify both data sets. Furthermore, the product of the precisions of every individual classification and the output of the change map of two classifications generally have identical precisions. Other constraints include the necessity for classifying products to be created using knowledge, experience, and time (Lu et al., 2004).

Other studies have been based on the classification process of Cellular automata. Cellular automata are computer-based “self-centered” modeling tools for which we consider the recording of the behaviors of individuals of elementary spatial entities called “cells” (Corgne, 2004). Space is represented by a grid of structured cells on which evolution rules are defined according to the principle of spatial and temporal auto-correlation. For example, the principle of the “Spacelle” model is adapted to the treatment of landscape evolution and environmental simulations. The spatialization of the cells around the central cell can be done according to a four-neighbor topology, the von Neumann neighborhood, or an eight-neighbor topology, called the Moore neighborhood. To the cells of the four cardinal points (North, East, South, West), Moore’s rule adds the intermediate cells which are those of the North-East, South-East, South-West and North-West. The interest

of this neighborhood in the dynamics of land occupation lies in the fact that considers all directions, especially when there are no obstacles (Dubos-Paillard et al., 2004; Langlois, 2001).

Among the various models and approaches that have been developed, some commonly used statistical techniques are based on the Markov field model (MRF). Our attention is focused on Markov random fields as a classification tool, because in recent years, MRF has become more and more popular, especially in image processing. Several reasons have led to the adoption of Markov fields a research mode. One of these is the growing attention to the role of spatial context in the classification of images, whereby a label with pixels or groups of pixels is allocated (Kato et al., 1994). In semantic segmentation in remote sensing, the Markov random field paradigm has gotten a lot of attention. In image processing, classification entails assigning pixels in an image to the class to which they belong based on a set of criteria. MRF is a probability graph model that describes geographic neighborhood interactions between pixels using a statistical approach. The MRF model may successfully combine a given image’s semantic properties and spatial neighborhood interactions, reducing the influence of intraclass differences. The MRF model consists of two sub-models (Zheng & Yao, 2019). The first is a set of features that effectively extract and model different features using a likelihood function, which measures the probability of occurrence for the characteristics of a pixel. The label field is the second sub-model, which models spatial neighborhood interactions among pixel class labels using the Markov potential function and property to minimize pixel heterogeneity within the same object. The feature field likelihood function in the conventional MRF model can only examine pixel-based features. The potential label field function can simulate neighborhood spatial interactions in a small geographic context, such as 4 or 8 neighborhood pixels. Therefore, the classic MRF model has been expanded to include more complex structures across a larger area (Zheng et al., 2019). This study applied the classification by Markov random fields on the colored composites of multi-spectral images Landsat MSS from 1985, ETM + from 2003, and Sentinel-2 from 2021 Al-Hubail wetland. This model is able to segment grayscale, color and textured images properly.

In addition, the use of change detection approaches, based on remote sensing and geographical information systems, offers the possibility of monitoring the spread or shrinkage of LULC classes and promotes an understanding of their dynamics. Methods for detecting change are essentially based on a multi-temporal analysis of satellite images. A number of change detection techniques have been developed to assess LULC changes using satellite

data (Alwashe et al., 1993; Borak et al., 2000; Close, 2021; Coppin et al., 2004; Lu et al., 2004; Rokni et al., 2015). The results are of great importance for wetland management decision-making and for predicting likely future development scenarios.

Materials and Methods

Study Area and Data

To offset water losses from the Al-Ahsa Oasis irrigation and drainage project in eastern Saudi Arabia, project management developed a strategy based on the use of non-traditional water sources such as treated wastewater and the reuse of agricultural drainage water while reducing groundwater pumping from wells. Excess agrarian drainage water is discharged into two wetlands: Al-Asfar and Al-Hubail, which were originally two sabkhas wetlands. Al-Hubail wetland is connected to the D1 canal of the Saudi Irrigation Organization (Fig. 1).

The wetland has a variety of natural environments (temporary pools, open ground, sand dunes, etc.), with ecosystems of great biological and ecological interest, which, thanks to the presence of water, allow the

permanent and temporary settlement of exceptional flora (macrophytes, algae, riparian vegetation, etc.) and fauna (*Tachybaptus ruficollis*, *Rallus aquaticus*, *Himantopus himantopus*, *Egretta garzetta*, *Circus aeruginosus*, *Accipiter nisus*, etc.). The site is one of the first refuges for waterfowl in the Arabian Peninsula, and one of their resting and feeding places. It attracts visitors, especially in winter, to enjoy the natural landscape and observe migratory birds. The birds migrate from cooler regions to areas with warmer climates, including the Al-Hubail wetland. However, the wetland water is now contaminated with heavy metals, mainly from agricultural wastewater. The level of heavy metals is generally higher than the international permissible limits and fluctuates seasonally (Alfarhan, 1999; Al-Taher, 1999; Ashraf et al., 2020; Fahmy et al., 2011; Salih, 2018); (Fig. 2).

In order to assess the evolution of the Al-Hubail wetland, two Landsat images (MSS from 1985 and ETM + from 2003) and one Sentinel-2 image (2021) were used for this analysis. All three images were acquired in the same season to avoid confusion in classification due to phenological changes. Because the area is often marshy and flooded in the wet season and dry in the summer, satellite imagery from the summer season (July and August) was primarily used to extrapolate the diverse land covers

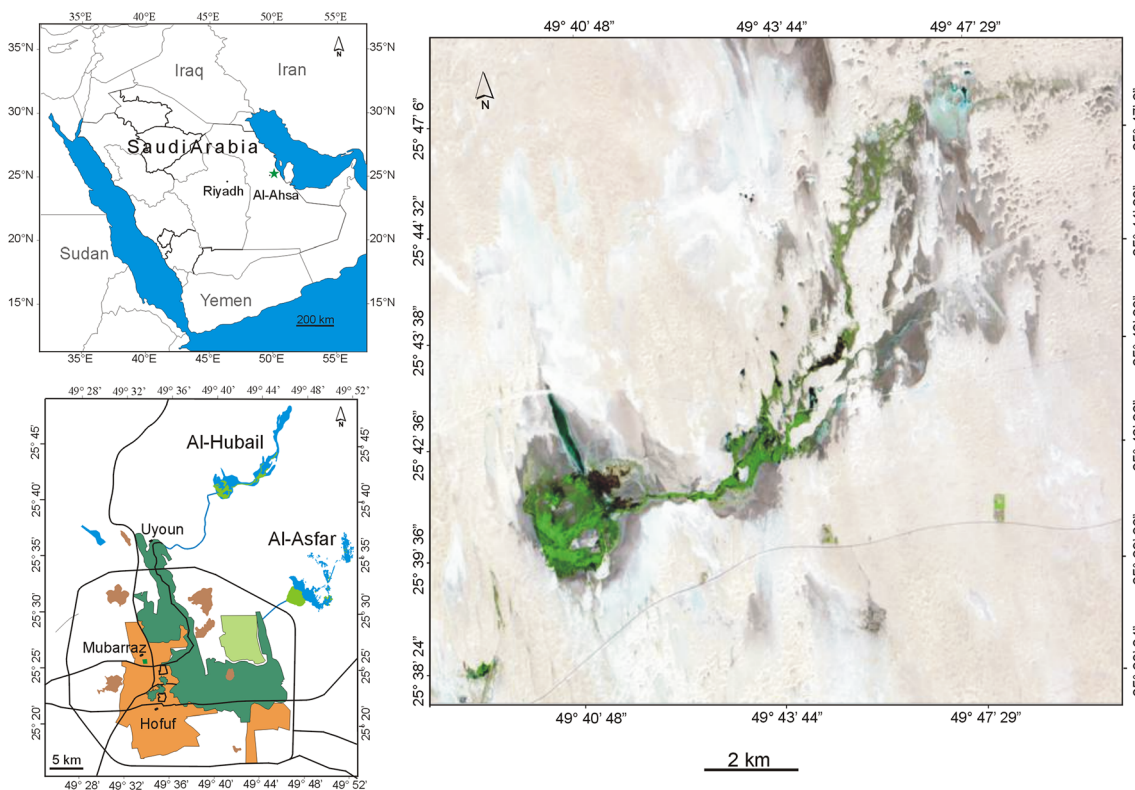


Fig. 1 Geographical location of the Al-Hubail wetland (eastern Saudi Arabia)

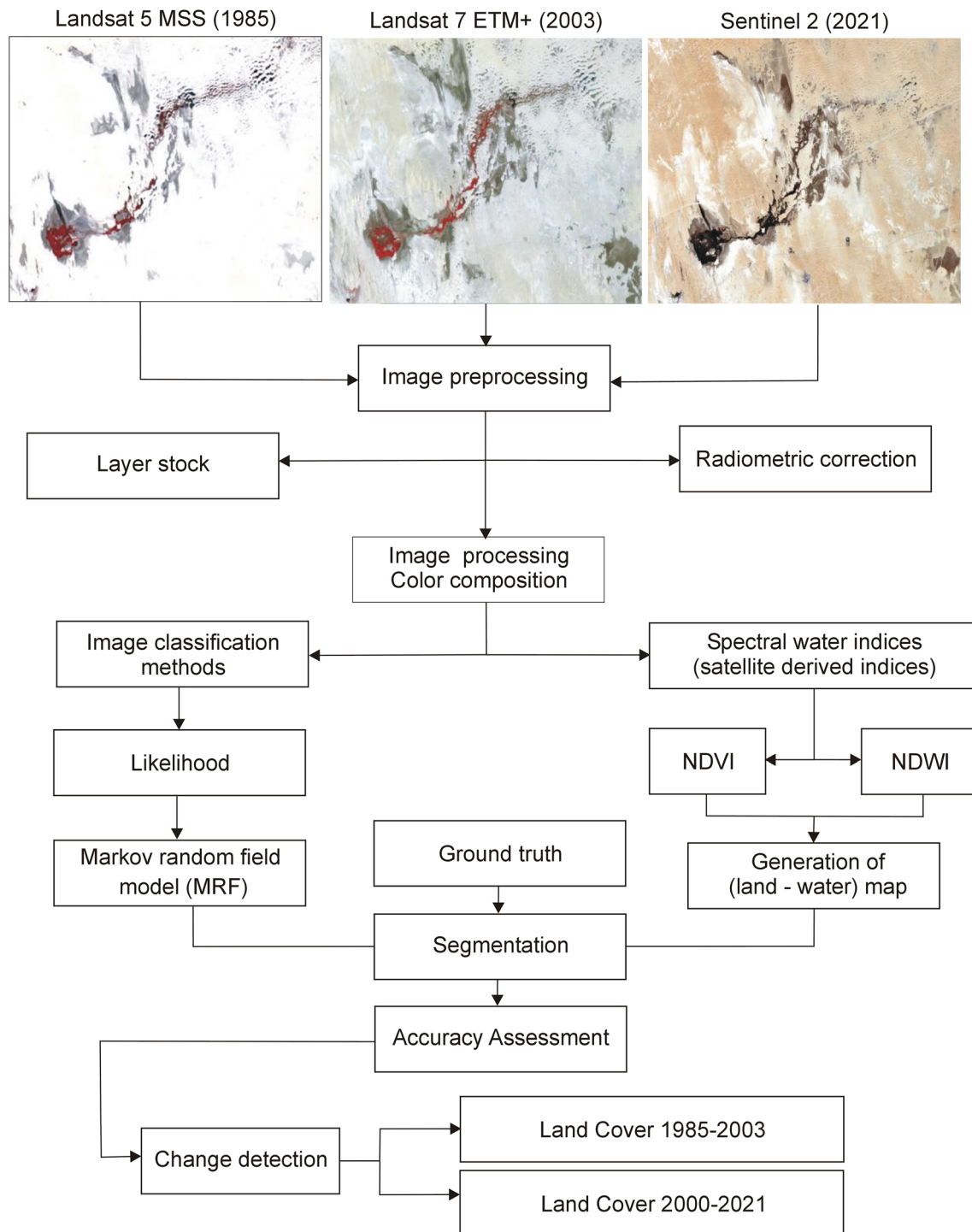


Fig. 2 The flow chart of the applied methodology

clearly. The land cover maps generated due to the classifications of the satellite images were then used for the spatiotemporal comparison. All data and information used in this study can be found in Table 1.

Classification of Satellite Images

The chosen satellite images underwent preliminary processing, during which radiometric and geometric adjustments were made (Fontinovo et al., 2012; Nguyen, 2015; Wang et al., 2012). This included radiometric calibrations

Table 1 All inputs for the classification of images in 1985, 2003 and 2021 (United States Geological Survey, 2022)

Images	Bands and features	Wavelength (μm) and description	Resolution (m)
Landsat 5 (MSS) 1985	Band 1 – Visible Green	0.5–0.6	60
	Band 2—Visible Red	0.6–0.7	60
	Band 3—NIR	0.7–0.8	60
	Band 4—NIR	0.8–1.1	60
	NDVI (Normalized Difference Vegetation Index)	(B 4 – B3) / (B4 + B3) (Near-Infrared – Visible) / (Near-Infrared + Visible)	60
	NDWI (Normalized Difference Water Index)	(B4 – B5) / (B4 + B5) Near-Infrared—Short-wave Infrared) / (Near-Infrared + Short-wave Infrared)	60
Landsat 7 (ETM +) (2003)	Band 1 – Visible	0.45–0.52	30
	Band 2—Visible	0.52–0.60	30
	Band 3—Visible	0.63–0.69	30
	Band 4—Near-Infrared	0.77–0.90	30
	Band 5—Short-wave Infrared	1.55–1.75	30
	Band 6—Thermal	10.40–12.50	60 (30)
	Band 7—Mid-Infrared	2.09–2.35	30
	Band 8—Panchromatic	0.52–0.90	15
	NDVI (Normalized Difference Vegetation Index)	(B 4 – B3) / (B4 + B3) (Near-Infrared – Visible) / (Near-Infrared + Visible)	30
	NDWI (Normalized Difference Water Index)	(B4 – B5) / (B4 + B5) (Near-Infrared—Short-wave Infrared) / (Near-Infrared + Short-wave Infrared)	30
Sentinel-2 (2021)	Band 1—Ultra blue (Coastal and Aerosol)	0.421–0.457	60
	Band 2—Blue	0.439–0.535	10
	Band 3—Green	0.537–0.582	10
	Band 4—Red	0.646–0.714	10
	Band 5—Visible and Near Infrared (VNIR)	0.694–0.714	20
	Band 6—Visible and Near Infrared (VNIR)	0.731–0.749	20
	Band 7—Visible and Near Infrared (VNIR)	0.768–0.796	20
	Band 8—Visible and Near Infrared (VNIR)	0.767–0.808	10
	Band 8A—Visible and Near Infrared (VNIR)	0.848–0.881	20
	Band 9—Short-Wave Infrared (SWIR)	0.931–0.958	60
	Band 10—Short-Wave Infrared (SWIR)	1.338–1.414	60
	Band 11—Short-Wave Infrared (SWIR)	1.539–1.681	20
	Band 12—Short-Wave Infrared (SWIR)	2.072–2.312	20
	NDVI (Normalized Difference Vegetation Index)	(B8—B4) / (B8 + B4) (NIR—RED) / (NIR + RED)	10
NDWI (Normalized Difference Water Index)	(B8—B12) / (B8 + B12) (NIR—MIR) / (NIR + MIR)		

to allow the transition from grayscale to apparent reflectance, the parameters of which were taken from the metadata of each image. After the geometric correction of these images, the boundary of the study area was digitized to crop the satellite images and extract the area of interest. Moreover, all the field work was carried out with the help of instruments like Differential Global Positioning System (DGPS), topographic maps, and digital cameras. The exact location of each area representing each land cover has to be determined. These areas are called training areas. They were used to classify the satellite images and evaluate their accuracy (Table 2).

After pre-processing the images and deriving NDVI and NDWI features, the images are classified utilizing Markov random field model (MRF) to produce land cover maps of the study area (Girard & Girard, 2010). Markovian modeling of the image is a probabilistic modeling based on a property of the images, namely the local interactions between neighboring gray levels to define the different regions of the image. In this study, we used during this study, we worked with an image modeled by Markov random fields and the Potts energy model using the simulated annealing (SA) algorithm. More often, for this model, the labels can represent a classification of the image. The MRF model takes advantage of spatial class dependencies (spatial context) among neighboring pixels in an image, and temporal class dependencies between different images of the same scene. The use of Markov fields makes it possible to consider the property of influence of the neighborhood of a point on the latter and to therefore insist on the coherence between the class of a pixel and that of its neighbors allowing to regularize the classification of satellite images. According to Solberg et al. (1996), when GIS field boundary data are included in the MRF model, the classification accuracy of the MRF model improves by 8%. For the detection of changes in agricultural areas, 75% of real class changes are identified by the MRF model, against 62% for the reference model.

After selecting the channels to be subjected for the classification, training areas were selected by digitizing polygons of sufficiently large and homogeneous zones. Based on the knowledge of the terrain, the plots were located on each candidate image for classification. Their outlines were delineated, avoiding the edge pixels to limit the variability within the plots. This was done to

distinguish the following land uses on the satellite images: Water bodies, hydromorphic areas, vegetation, and open ground. The training plots were evaluated using a contingency matrix representing the confusion between the classes used for classification. This matrix was used to redefine these areas to avoid such confusion as much as possible.

Evaluation of the Detection of Changes

Change detection techniques assume that a change in surface coverage results in a corresponding change in reflectance. Recently, many change detection techniques have been developed. Unsupervised Markov random field (MRF) methods help detect changes in remote sensing images (He et al., 2015). Markov random field (MRF) uses spectral and spatial data in image processing (Gong et al., 2014). MRF uses the maximum a posteriori (MAP) criterion to take full advantage of the spectral properties of pixels and the label field characteristic of their neighborhoods to offer the best image analysis results (Gu et al., 2017). Several approaches have been implemented for the difference image generated by the change vector analysis (CVA) method. MRF combines spectral and spatial CVA data efficiently. A custom-designed Potts model was developed to improve the accuracy of spatial information weights (Hao et al., 2014).

When the Potts model is used to estimate the energy of the label field in MRF, the weights adopted for each pixel in the differential pictures are the same, regardless of the gray value distribution of the pixels. Each pixel in a differential image has its unique grayscale value and, consequently, its unique probability of being altered. When the gray value of a pixel is high, there is a greater probability that it will change; on the other hand, when the gray value is low, there is a greater probability that it will not change. If you merely observe at the gray value, it can be challenging to determine whether or not there has been a change in pixels with an intermediate gray level. In the standard implementation of the Potts model, each pixel in differential images is assigned the same penalty coefficient when it is defined. This setting frequently results in neighborhood spatial information, which leads to an excessive amount of smoothing on areas that have been adjusted for pixels with extraordinarily high or low gray

Table 2 Data collected during training and testing for all images

Images' year	Water bodies		Vegetation		Hydromorphic areas		Open ground	
	Train	Test	Train	Test	Train	Test	Train	Test
1985	40	80	45	91	53	88	40	115
2003	52	89	57	110	61	120	49	120
2021	38	68	53	115	72	120	40	92

values (Gu et al., 2017). Since it considers the temporal aspect of the information, the proposed model is appropriate for identifying the class changes among the dates on which the multiple images were taken.

In the next step, a geographic information system-based overlay technique was applied to obtain the spatial changes in land cover over two time periods: 1985–2003 and 2003–2021. For each of the three four-class maps, a new thematic layer was created with different combinations of change classes. The result of this technique is a cross-matrix with two entries that describes the main types of changes in the studied area.

Spectral Bands and Features Used for the Classification

The maps in Figs. 3, 4 and 5 are the results of the classification of MSS multi-spectral images from 1985, ETM + from 2003 and Sentinel-2 from 2021 by a Markov field using the Potts model method as the sampling method.

Due to the presence of water and vegetation in the study area and in order to obtain a very accurate classification, the Normalized Difference Vegetation Index (NDVI) and the Normalized Difference Water Index (NDWI) were added outside the spectral band of the satellite imagery according to the following formulas as input to the classification algorithm (Fig. 3a–c and Fig. 4a–c).

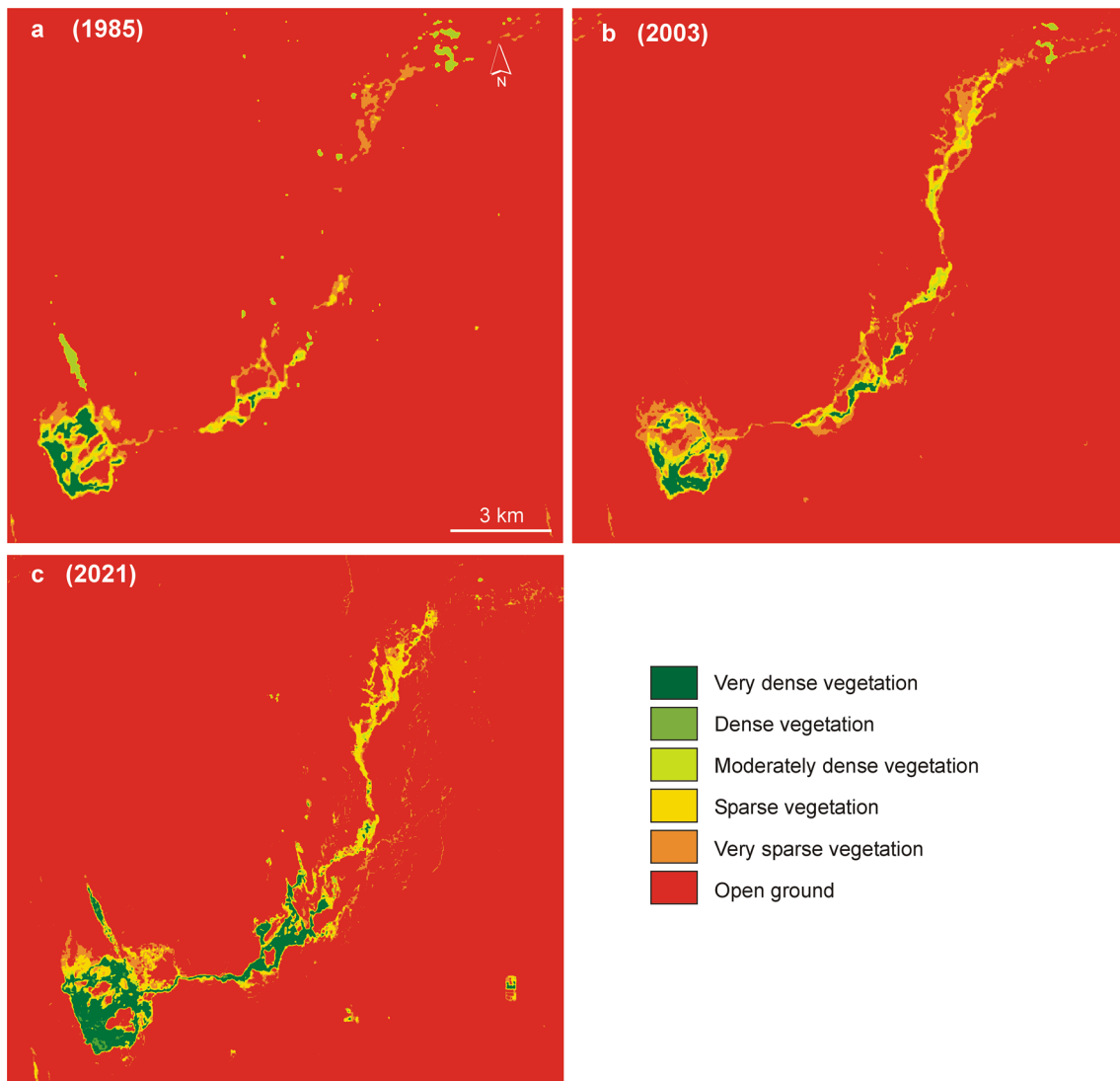


Fig. 3 a–c NDVI

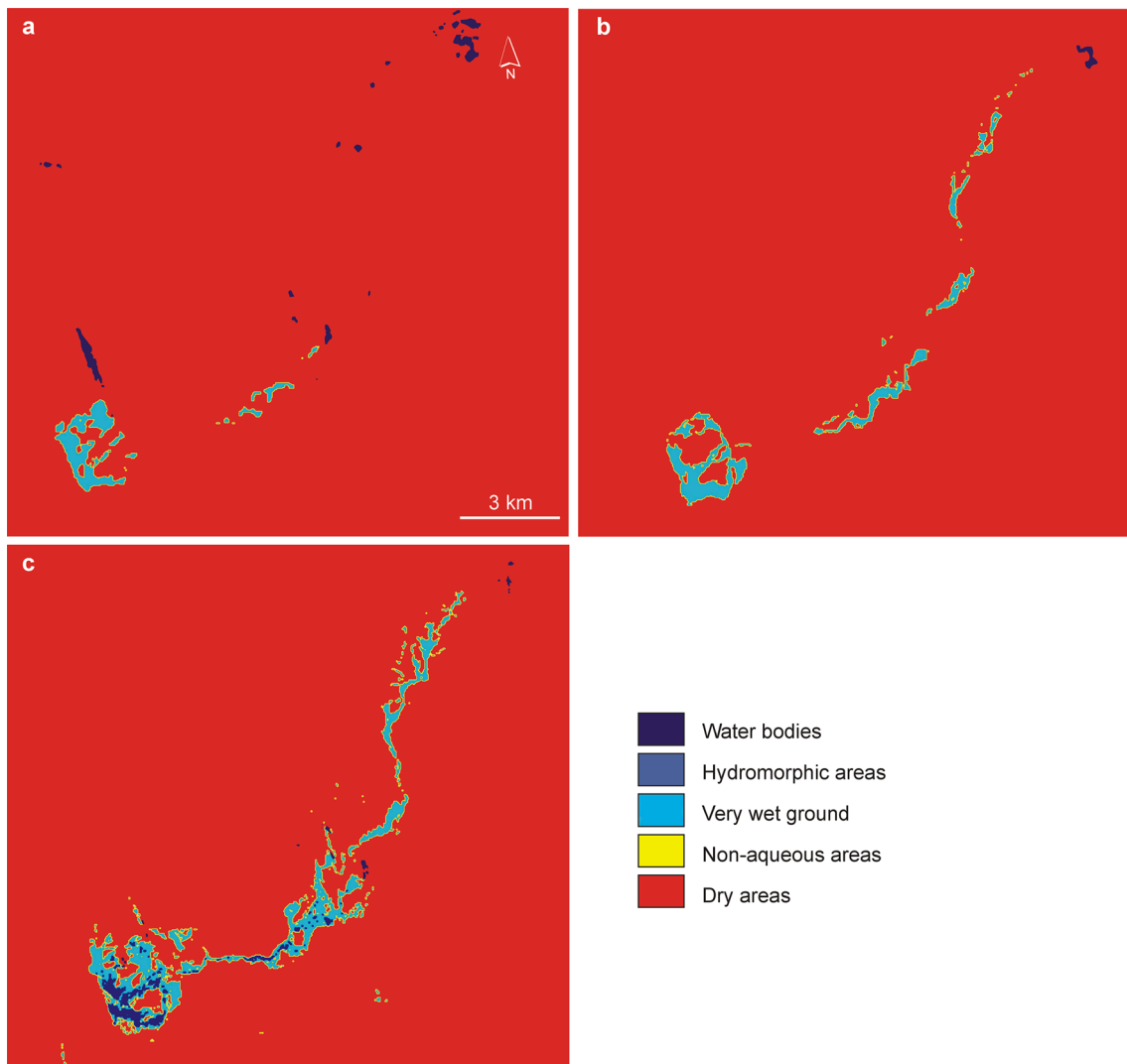


Fig. 4 a–c NDWI

$$\text{NDVI} = \frac{X_{\text{NIR}} - X_{\text{SWIR}}}{X_{\text{NIR}} + X_{\text{SWIR}}}$$

$$\text{NDWI} = \frac{X_{\text{Green}} - X_{\text{NIR}}}{X_{\text{Green}} + X_{\text{NIR}}}$$

Figures 3a–c and 4a–c show the NDVI and NDWI derived for each satellite images. In combination with the spectral bands of the satellite images, these extracted indices allow the classification of each image. Table 1 provides information on all spectral bands and indices that contributed to the classification of the 1985, 2003, and 2021 images.

Results and Discussion

The Markov random field (MRF) method is used to detect changes after creating the classification maps. The results of this classification were compared with the accuracy of

the land cover maps and topographic maps. The findings of land cover classification and change detection are introduced in this section.

Validation of Land Cover Maps

The extraction of training data, the creation and training of the classifier model, and, finally, the assessment of the accuracy of the maps utilizing the test data are the three processes in the image classification and generation of land cover maps procedure. The number and technique of collecting training and testing data affect the classification and change detection quality in the first and third steps of this process. Satellite image classification is used to detect changes. Thus, in order to assess the producer's accuracy, Petropoulos et al., (2015) showed the importance of generating ground truth points using the random sampling method. For this reason, in this work, the collection of

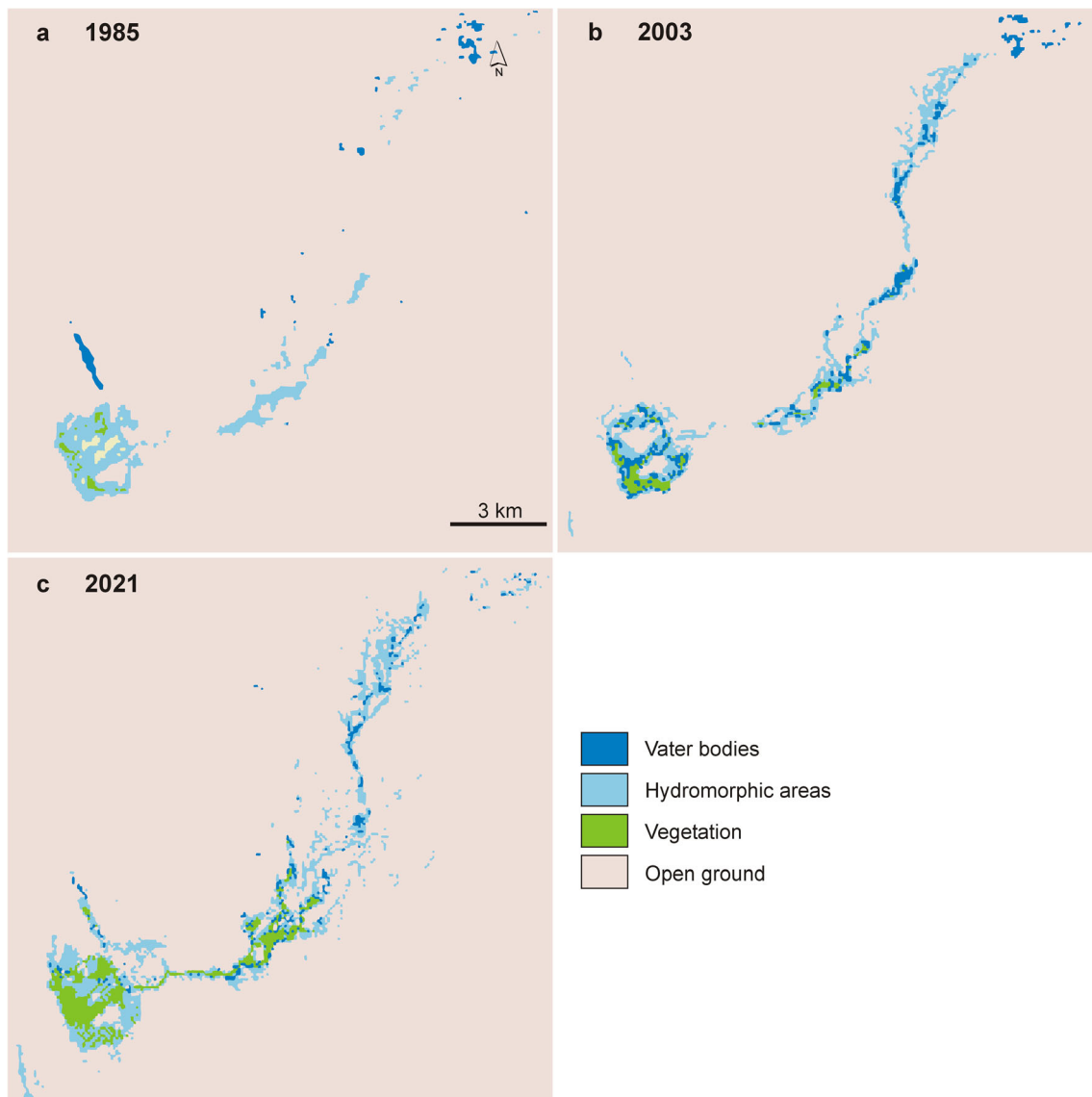


Fig. 5 a–c Maps of land cover

training and testing data was not only done by field surveys, but DGPS and satellite imagery were also used in this step to collect very reliable data. Table 2 shows the number of training and test data extracted to train the classifier and evaluate the accuracy of the maps produced in 1985, 2003, and 2021 (Fig. 5a–c).

The derived land cover maps for 1985, 2003, and 2021 are shown in Figs. 5a–c. The extent of hydromorphic area

and vegetation classes can be visually seen on these maps. Table 3 shows the confusion matrix for the classification maps (Table 3).

The four land cover classes each have a distinct spectral behavior in all the satellite images used: water bodies, vegetation, hydromorphic areas and open ground. Also, the comparison between the three contingency matrices created for the years 1985, 2003, and 2021 shows a constant

Table 3 Average contingency matrix for the three satellite images of 1985, 2003, and 2021 (in %)

Classes	Water bodies	Hydromorphic areas	Vegetation	Open ground
Water bodies	90.3	6.8	2.3	1.6
Hydromorphic areas	6.2	84.9	3.2	4.8
Vegetation	2.4	4.8	90.1	3.1
Open ground	1.1	3.5	1.2	90.5

improvement in the separability of the land cover classes. V. A. Tolpekin and A. Stein (2009) explore the results of class separability in super-resolution mapping on the basis of Markov random fields (MRF). The authors systematically varied the separability of the classes, the scale factor, and the smoothing parameters' significance. The accuracy of the generated land cover map is evaluated using the kappa statistic at the fine resolution scale and the class area proportion at the coarse resolution scale. According to the research findings, MRF may now be used for more extensive images, and the class separability can range anywhere from poor to excellent.

The Accuracy Rating Estimator is the final step in the image classification process (Foody, 2002). It is a question of quantitatively evaluating the efficiency with which the pixels were sampled by the Markov random field's method. There are different accuracy assessment models like the accuracy assessment methods including the standard kappa coefficient, overall accuracy, producer's accuracy and user's accuracy. The overall accuracy estimator calculates the number of pixels classified accurately in the image. Validation of the classification consists of a statistical test supported by a field visit (Nguyen, 2015; Petropoulos et al., 2015). Markov random field correctly discriminates the different classes of land use with the highest accuracy for a 2021 map derived from Sentinel-2 processing with a kappa coefficient of 0.9 and a total accuracy of 91.5, followed by a 2003 map derived from image processing of ETM + sensors with a kappa coefficient of 0.88 and a total accuracy of 90.6, which verifies the effectiveness of the proposed MRF model. The average accuracy resulting from the combination of the four confusion matrices developed for the three land cover maps is 88.9%. In addition, the user's accuracy measures how often the class on the map is actually present on the ground. The producer's accuracy measures the number of pixels classified to a class that accurately fits in to that class only (Patel & Kaushal., 2010). A wide-field survey was performed and Sentinel-2 images were used to collect ground truth (validation) data for 2021. The user's accuracy ranged from 81.3 to 91.4%, while the producer's accuracy ranged from 84.3 to 94.8%. Table 4 shows the producer and user's accuracy.

Taking into account the local interactions between each pixel with the neighboring pixels made it possible to define the different zones of the image. This advantage has made it possible to obtain results reflecting the reality of the field with an overall precision greater than 0.88, thus improving the image classification process.

However, Gu et al., (2017) use an improved MRF to detect changes. MRF uses linear weights to split unchanged, uncertain, and modified pixels to improve spatial database precision. Test results demonstrate the proposed method can improve change detection accuracy. The recommended method can provide a change detection image closer to ground reference data, resulting in higher accuracy and more accurate conclusions than classic MRF methods that use the Potts model. While Zheng et al., (2019) proposed an object-based Markov random field model with an anisotropic penalty matrix. The suggested method could boost overlay accuracy (OA) and kappa values by considering anisotropy between classes. The suggested OMRF-AP model improved segmentation accuracy on high spatial resolution remote sensing images by 4 percent on average and 10 percent on OA and kappa.

Change Detection Results

To determine the extent of land cover change in the Al-Hubail wetland, a geographic information system (GIS) was overlaid to detect the differences between 1985 and 2003 in Fig. 6a and between 2003 and 2021 in Fig. 6b. The change maps are shown in Fig. 6a–b and show significant changes in the land cover of the study area.

Table 5 shows the area occupied by each land cover class. Analysis of this table shows a significant increase in hydromorphic areas and vegetated areas over 36 years. Hydromorphic areas have increased from 7.91 km² (2.69%) to 7.62 km² (2.85%) from 1985 to 2003 and to 20.05 km² (6.82%) by 2021.

Figure 7 shows the percent change in each land cover between 1985 and 2021. Figure 7 shows different trends for each land cover. Wetlands comprised about 1.4% of the study area in 1985 and then increased sharply to over 6.8% in 2021. Despite the ongoing conflict between water and sand in the area, the area of wetlands (aquatic and hydromorphic) gradually increased from about 4.09% in 1985 to

Table 4 Evaluation of accuracy resulting from satellite image processing

Classes	Producer's accuracy (%)			User's accuracy (%)		
	1985	2003	2021	1985	2003	2021
Water bodies	89.1	92.3	94.6	88.2	91.3	91.4
Hydromorphic areas	84.3	88.9	89.8	81.3	86.2	87.4
Vegetation	91.6	90.8	94.8	90.6	89.5	90.1
Open ground	85.1	88.3	90.7	90.1	90.2	91.4

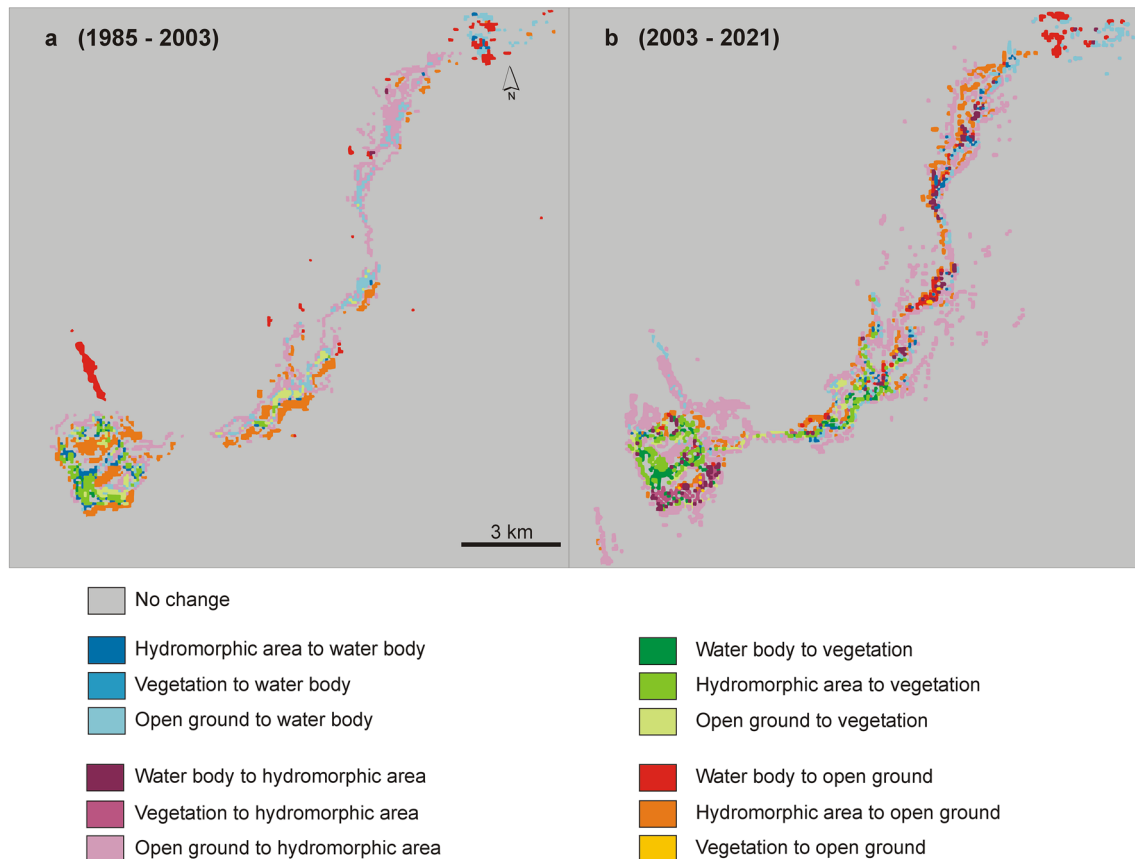


Fig. 6 a–b Change detection maps

Table 5 Area coverage of land cover classes for the study area from 1985 to 2021

Classes	1985		2003		2021	
	Km ²	%	Km ²	%	Km ²	%
Water bodies	4.12	1.4	6.95	2.36	3.71	1.26
Hydromorphic areas	7.91	2.69	8.37	2.85	20.05	6.82
Vegetation	1.72	0.55	2.83	0.96	6.82	2.32
Open ground	280.18	95.32	275.78	93.83	263.35	89.59
Total	293.93	100	293.93	100	293.93	100

5.21% in 2003 and then rapidly increased to nearly 12% in 2021. The vegetated area also increases gradually from 0.38% to 2.32% between 1985 and 2021. Overall, there is a strong trend of increasing water and vegetated areas between 1985 and 2021. At the same time, there is a strong decrease in open ground area, which is related to an increasing input of drainage water into the Al-Hubail depression (Fig. 7). This same dynamic was detected by Chouari (2021b), studying the evolution of the Al-Asfar wetland to the east of Al-Ahsa Oasis. The author indicates that the wetland area has increased significantly for the past three decades. The changes detected in the study area can be explained by the discharge of agricultural drainage water and semi-treated water from sewage treatment plants.

According to Mccauley (2015), tracking semi-permanent and permanent wetlands in the Prairie Pothole region of North Dakota, the USA, showed that water bodies represent 86% higher in wetlands than they were historical. The differences can be attributed to consolidation drainage, which has decreased the abundance of aquatic invertebrates and changed the land cover of these wetlands.

Tables 6 and 7 show the result of the contingency table. They summarize the main changes in land cover during the periods 1985–2003 and 2003–2021.

As shown in Table 6, most hydromorphic areas increased in size (about 2.80 km² and 9.89 km², respectively) due to the conversion of previously open ground areas.

Fig. 7 Evolution of land cover in the Al-Hubail wetland (1985–2021)

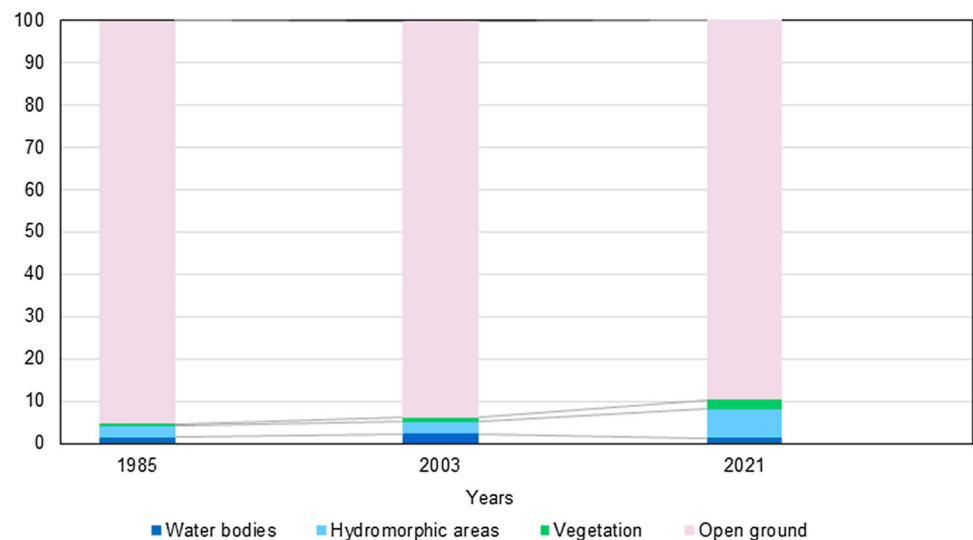


Table 6 Details of the change in wetland area between 1985 and 2003 in km²

Classes		1985			
		Water bodies	Hydromorphic areas	Vegetation	Open ground
2003	Water bodies	2.49	0.57	0.21	3.68
	Hydromorphic areas	0.32	3.74	1.31	2.80
	Vegetation	0.29	0.90	0	1.64
	Open ground	0.92	2.33	0.34	272.19

Table 7 Details of change in wetland area between 2003 and 2021 in km²

Classes		2003			
		Water bodies	Hydromorphic areas	Vegetation	Open ground
2021	Water bodies	2.48	0.37	0.65	0.21
	Hydromorphic areas	3.46	3.91	2.79	9.89
	Vegetation	0.79	1.02	0	5.01
	Open ground	1.12	2.29	0.13	259.81

A huge transformation between vegetation and hydromorphic areas (1.02 km²) also occurred between 2003 and 2021. As shown in Table 7, the conversion of approximately 5.01 km² of open ground resulted in a vegetated area.

The results show that methods based on the Markov random field (MRF) are effective methods for detecting changes in remote sensing images. Several variants of Markov models have been developed, like Markov chain, Markov trees, Coupled hidden Markov models, Dempster-Shafer theory or that fuzzy logic (Chen & Cao, 2013; Gong et al., 2014; Gu et al., 2017; Hao et al., 2014; He et al., 2015; Pieczynski, 2003). These Markovian models have significantly improved image classification results, yielding good results. Unlike these works, our model was applied to Landsat MSS, ETM + and Sentinel-2 images and the results are satisfactory and reflect the reality of the field.

Markov models are tools to solve the problem of uncertainty and imprecision contained in images. In image processing, this type of method's success is due to their ability to produce satisfactory results, when the various noises present in the image considered are significant and when the data correspond well to the model used. The Markov fields used in this study for the classification of Landsat MSS, ETM + and Sentinel-2 images have been used by several authors in previous researches for the same image classification objective. The advantage of the Markov field model in image processing compared to so-called "local" models is its ability to take into account all the information available on the observed image (Pieczynski, 2003).

However, the classic label field cannot accurately identify the spatial relationships between neighboring pixels. Studies often develop a change detection method

based on an improved MRF to solve these problems. However, the classic label field could not identify spatial relationships between pixels. To address these difficulties, researchers often use an upgraded MRF. Due to imprecision in identifying neighbor pixel relationships and determining weights, MRF spatial information cannot be utilized entirely (Chen & Cao, 2013). Inaccurate spatial relationships and spatial information weights result in an overly smooth change map. MRF must balance detail preservation with denoising.

In addition, the spatial neighborhood link between pixels in the classic Potts model is typically defined as either 0 or 1, which is too absolute and imprecise. This method has a propensity for making excessive use of spatial data and smoothing out the change detection maps (Gu et al., 2017). It is recommended that advanced MRF models be provided in research to overcome these limitations. This will ensure more incredible performance with less overall error detection and more resilient performance to parameter change. According to He et al. (2015), to improve the detail preservation capabilities of MRF, the local uncertainty in a particular window is first evaluated. Then, it is integrated into the spatial energy term of the MRF model. This is done to raise the MRF's capabilities. The proposed local uncertainty MRF (LUMRF) method produces a refined change map. According to the findings, in comparison to MRF, LUMRF offers superior performance with lower overall error detection and is more resistant to parameter changes.

Conclusion

This study aimed to record and analyze the land cover changes in the Al-Hubail wetland in northeastern Al-Ahsa, eastern Saudi Arabia. The study area has changed dramatically during the last two decades due to various reasons, such as the discharge of increasing amounts of irrigation water into the wetland. Multi-spectral and temporal satellite images (Landsat 5 MSS, Landsat 5 ETM + and Sentinel-2) from 1985, 2003 and 2021 were used to achieve this objective. After pre-processing the satellite images and in order to achieve a highly accurate classification, the water and vegetation indices (NDVI and NDWI) were integrated with the spectral bands of the satellites and used as input for the classification process. To classify the images and generate land cover maps for different selected years, a Markov random field (MRF) with the Potts energy model is used to analyze the land cover between 1985 and 2003 and 2003–2021. We were interested in a classification integrating the spatial constraint in the approaches of classification of the multi-spectral images by using the fields of Markov. The success of this type

of method is due to its ability to produce, when the various noises present in the image are significant, and when the data correspond well to the model used, important results. The integration in the classification process of the spatial constraint which resulted in taking into account the local interactions between each pixel with the neighboring pixels made it possible to define the different parts of the image. This advantage has made it possible to obtain results reflecting the reality of the field with an overall precision greater than 0.9, thus improving the image classification process.

In general, the results showed a remarkable change within the Al-Hubail wetland and its surroundings between 1985 and 2021. The most significant change was found in the hydromorphic area class, which increased from 2.32 km² in 1985 to 9.89 km² in 2021 at the expense of the open ground class. This study expresses that remote sensing and GIS are important technologies for the temporal analysis of environmental phenomena that would otherwise not be possible with obsolete techniques. With these technologies, it is now possible to detect changes more accurately, quickly, and at a lower cost.

Acknowledgments The following statement must be included in the article: This work was supported by the Deanship of Scientific Research, Vice Presidency for Graduate Studies and Scientific Research, King Faisal University, Saudi Arabia [Grant No. 831].

Declarations

Conflict of Interest The author declares that he has no known competing financial interests or personal relationships that could have appeared to influence the work reported in this paper.

References

- Abdel-Moneim, A. (2014). Histopathological and ultrastructural perturbations in tilapia liver as potential indicators of pollution in Lake AlAsfar, Saudi Arabia. *Environmental Science and Pollution Research*, 21, 4387–4439. <https://doi.org/10.1007/s11356-013-2185-9>
- Al-Dakheel, Y. Y., Hussein, A. H. A., El-Mahmoudi, A. S., & Massoud, M. A. (2009). Soil, water chemistry and sedimentological studies of Al Asfar evaporation lake and its Inland sabkha, Al-Hassa area, Saudi Arabia. *Asian Journal of Earth Sciences*, 2, 1–21. <https://doi.org/10.3923/ajes.2009.1.21>
- Alfarhan, A. H. (1999). A phytogeographical analysis of the floristic elements in Saudi Arabia. *Pakistan Journal of Biological Sciences*, 2, 702–711. <https://doi.org/10.3923/pjbs.1999.702.711>
- Al-Hussaini, Y. A. (2005). The use of multi-temporal landsat TM imagery to detect land cover/use changes in AlHassa, Saudi Arabia. *Scientific Journal of King Faisal University (basic and Applied Sciences)*, 6(1), 1426.
- Almadini, A. M., & Hassaballa, A. A. (2019). Depicting changes in land surface cover at AlHassa oasis of Saudi Arabia using remote sensing and GIS techniques. *PLoS ONE*, 14(11), e0221115. <https://doi.org/10.1371/journal.pone.0221115>

- Almutairi, A., & Warner, T. A. (2010). Change detection accuracy and image properties: A study using simulated data. *Remote Sensing*, 2, 1508–1529. <https://doi.org/10.3390/rs2061508>
- Al-Obaid, S., Samraoui, B., Thomas, J., El-Serehy, H. A., Alfarhan, A. H., Schneider, W., & O'Connell, M. (2017). An overview of wetlands of Saudi Arabia: Values, threats, and perspectives. *Ambio*, 46, 98–108. <https://doi.org/10.1007/s13280-016-0807-4>
- Al-Sheikh, H., & Fathi, A. A. (2010). Ecological studies on Al-Asfar lake. Al-Hassa, Saudi Arabia, with special references to the sediment. *Research Journal of Environmental Sciences*, 4, 13–22. <https://doi.org/10.3923/rjes.2010.13.22>
- Al-TaHER, A. A. (1999). *Al-Hassa: Geographical studies* (pp. 1–385). King Saud University.
- Alwashe, M. A., & Bokhari, A. Y. (1993). Monitoring vegetation changes in Al Madinah, Saudi Arabia, using thematic mapper data. *International Journal of Remote Sensing*, 14, 191–197. <https://doi.org/10.1080/01431169308904331>
- Ashraf, M. Y., Al-Fredan, M. A., & Fathi, A. A. (2020). Floristic composition of lake Al-Asfar, Alahsa, Saudi Arabia. *International Journal of Botany*, 5, 116–125.
- Asselen, S. V., Verburg, P. H., Vermaat, J. E., & Janse, J. H. (2013). Drivers of wetland conversion: A global meta-analysis. *PLoS ONE*, 8(11), e81292. <https://doi.org/10.1371/journal.pone.0081292>
- Borak, J. S., Lambin, E. F., & Strahler, A. H. (2000). The use of temporal metrics for land-cover change detection at coarse spatial scales. *International Journal of Remote Sensing*, 21(6–7), 1415–1432. <https://doi.org/10.1080/014311600210245>
- Chen, J., Gong, P., He, C., Pu, R., & Shi, P. (2003). Land-use/land-cover change detection using improved change-vector analysis. *Photogrammetric Engineering and Remote Sensing*, 69(4), 369–379.
- Chen, Y., & Cao, Z. (2013). An improved MRF-based change detection approach for multitemporal remote sensing imagery. *Signal Processing*, 93(1), 163–175.
- Chouari, W. (2021a). Contributions of multispectral images to the study of land cover in wet depressions of eastern Tunisia. *The Egyptian Journal of Remote Sensing and Space Sciences*, 24, 443–451. <https://doi.org/10.1016/j.ejrs.2020.11.003>
- Chouari, W. (2021b). Wetland land cover change detection using multitemporal Landsat data: A case study of the Al-Asfar wetland, Kingdom of Saudi Arabia. *Arabian Journal of Geosciences*, 14, 523. <https://doi.org/10.1007/s12517-021-06815-y>
- Close, O., Petit, S., Beaumont, B., & Hallot, E. (2021). Evaluating the potentiality of sentinel-2 for change detection analysis associated to LULUCF in Wallonia. *Belgium. Land*, 10(1), 55. <https://doi.org/10.3390/land10010055>
- Coppin, P., Jonckheere, I., Nackaerts, K., Muys, B., & Lambin, E. (2004). Review article digital change detection methods in ecosystem monitoring: A review. *International Journal of Remote Sensing*, 25, 1565–1596. <https://doi.org/10.1080/0143116031000101675>
- Corgne, S. (2004). Modélisation prédictive de l'occupation des sols en contexte agricole intensif : Application à la couverture hivernale des sols en Bretagne, « Predictive modeling of land use in an intensive agricultural context: Application to winter soil cover in Brittany ». Ph.D. Thesis, University of Rennes 2-Haute-Bretagne, France, 230 p
- Deng, J. S., Wang, K., Deng, Y. H., & Qi, G. J. (2008). PCA-based land-use change detection and analysis using multitemporal and multisensor satellite data. *IEEE International Geoscience and Remote Sensing Symposium*, 29, 4823–4838. <https://doi.org/10.1080/01431160801950162>
- Dubos-Paillard, E., Guermond, Y., & Langlois, P. (2004). Analyse de l'évolution urbaine par automate cellulaire, le modèle Spacelle analysis of urban evolution by cellular automata, the Spacelle model. *L'espace Géographique*, 32, 357–378.
- Eid, A. N. M., Olatubara, C. O., Ewemoje, T. A., Farouk, H., & El-Hennawy, M. T. (2020). Coastal wetland vegetation features and digital change detection mapping based on remotely sensed imagery: El-Burullus Lake. *Egypt. International Soil and Water Conservation Research*, 8(1), 66–79.
- El-Hattab, M. M. (2015). Change detection and restoration alternatives for the Egyptian lake Maryut Egypt. *The Egyptian Journal of Remote Sensing and Space Science*, 18(1), 9–16. <https://doi.org/10.1016/j.ejrs.2014.12.001>
- El-Hattab, M. M. (2016). Applying post classification change detection technique to monitor an Egyptian coastal zone (Abu Qir Bay). *The Egyptian Journal of Remote Sensing and Space Science*, 19(1), 23–36. <https://doi.org/10.1016/j.ejrs.2016.02.002>
- Fahmy, G. H., & Fathi, A. A. (2011). Limnological studies on the Wetland lake, Al-Asfar, with special references to heavy metal accumulation by fish. *American Journal of Environmental Sciences*, 7(6), 515–524. <https://doi.org/10.3844/ajessp.515-524>
- Fathi, A. A., Al-Fredan, M. A., & Youssef, A. M. (2009). Water quality and phytoplankton communities in Lake Al-Asfar, AL-Hassa, Saudi Arabia. *Research Journal of Environmental Sciences*, 3, 504–513. <https://doi.org/10.3923/rjes.2009.504.513>
- Fontinovo, G., Allegrini, A., Atturo, C., & Salvatori, R. (2012). Speedy methodology for geometric correction of MIVIS data. *European Journal of Remote Sensing*, 45(1), 19–25. <https://doi.org/10.5721/EuJRS20124502>
- Foody, G. M. (2002). Status of land cover classification accuracy assessment. *Remote Sensing of Environment*, 80(1), 185–201. [https://doi.org/10.1016/S0034-4257\(01\)00295-4](https://doi.org/10.1016/S0034-4257(01)00295-4)
- Gardner, R., Finlayson, M. (2018). *Global Wetland outlook: State of the World's Wetlands and their services to people*; Ramsar Convention: Gland, Switzerland.
- Girard, M. C., Girard, C. M. (2010). *Traitement des données de télédétection-2e éd. : Environnement et ressources naturelles*. Dunod, Paris, 576 p.
- Gong, M. G., Su, L. Z., Jia, M., & Chen, W. S. (2014). Fuzzy clustering with a modified MRF energy function for change detection in synthetic aperture radar images. *IEEE Transactions on Fuzzy Systems*, 22(1), 98–109. <https://doi.org/10.1109/TFUZZ.2013.2249072>
- Gu, W., Lv, Z., & Hao, M. (2017). Change detection method for remote sensing images based on an improved Markov random field. *Multimedia Tools and Applications*, 76(17), 17719–17734.
- Hao, M., Shi, W., Deng, K., & Zhang, H. (2014). A contrast-sensitive Potts model custom-designed for change detection. *European Journal of Remote Sensing*, 47(1), 643–654. <https://doi.org/10.5721/EuJRS20144736>
- He, P., Shi, W., Miao, Z., Zhang, H., & Cai, L. (2015). Advanced Markov random field model based on local uncertainty for unsupervised change detection. *Remote Sensing Letters*, 6(9), 667–676. <https://doi.org/10.1080/2150704X.2015.1054045>
- Hussain, M., Chen, D., Cheng, A., Wei, H., & Stanley, D. (2013). Change detection from remotely sensed images: From pixel-based to object-based approaches. *ISPRS Journal of Photogrammetry and Remote Sensing*, 80, 91–106. <https://doi.org/10.1016/j.isprsjprs.2013.03.006>
- Kato, Z. (1994). Modelisations Markovian multiresolutions in vision by computer: Application to the segmentation of image SPOT. Ph.D. Thesis, University of Nice, France.
- Langlois, P. (2001). Le modèle SpaCell. *Base de données du Groupe Modèles du GDR Libergéo*, 111–125
- Lu, D., Mausel, P., Brondizio, E., & Moran, E. (2004). Change detection techniques. *International Journal of Remote Sensing*, 25, 2365–2401. <https://doi.org/10.1080/0143116031000139863>

- Macleod, R. D., & Congalton, R. G. (1998). Quantitative comparison of change-detection algorithms for monitoring eelgrass from remotely sensed data. *Photogrammetric Engineering and Remote Sensing*, 64, 207–216.
- Maimaitijiang, M., Ghulam, A., Sandoval, J. O., & Maimaitiyiming, M. (2015). Drivers of land cover and land use changes in St. Louis metropolitan area over the past 40 years characterized by remote sensing and census population data. *International Journal of Applied Earth Observation and Geoinformation*, 35, 161–174. <https://doi.org/10.1016/j.jag.2014.08.020>
- Mccauley, L., Anteau, M., Post van der Burg, M., & Wiltermuth, M. (2015). Land use and wetland drainage affect water levels and dynamics of remaining wetlands. *Ecosphere*, 6, 1–22. <https://doi.org/10.1890/ES14-00494.1>
- Nemmour, H., & Chibani, Y. (2006). Multiple support vector machines for land cover change detection: An application for mapping urban extensions. *ISPRS Journal of Photogrammetry and Remote Sensing*, 61(2), 125–133. <https://doi.org/10.1007/s12524-011-0060-z>
- Nguyen, T. H. (2015). Optimal ground control points for geometric correction using genetic algorithm with global accuracy. *European Journal of Remote Sensing*, 48(1), 101–120. <https://doi.org/10.5721/EuJRS20154807>
- Ojaghi, S., Ahmadi, F. F., Ebadi, H., & Bainchetti, R. (2017). Wetland cover change detection using multi-temporal remotely sensed data a case study: Ghara Gheshlagh wetland in the southern part of the Urmia Lake. *Arabian Journal of Geosciences*, 10, 470. <https://doi.org/10.1007/s12517-017-3239-y>
- Patel, N., & Kaushal, B. (2010). Improvement of user's accuracy through classification of principal component images and stacked temporal images. *Geo-Spatial Information Science*, 13(4), 243–248. <https://doi.org/10.1007/s11806-010-0380-0>
- Petropoulos, G. P., Kalivas, D. P., Griffiths, H. M., & Dimou, P. P. (2015). Remote sensing and GIS analysis for mapping spatio-temporal changes of erosion and deposition of two Mediterranean river deltas: The case of the Axios and Aliakmonas rivers, Greece. *International Journal of Applied Earth Observation and Geoinformation*, 35, 217–228. <https://doi.org/10.1016/j.jag.2014.08.004>
- Pieczynski, W. (2003). Modèles de Markov en traitements d'images. *Traitement Du Signal*, 20(3), 255–278.
- Rapinel, S., Hubert-Moy, L., & Clément, B. (2015). Combined use of LiDAR data and multispectral earth observation imagery for wetland habitat mapping. *International Journal of Applied Earth Observation and Geoinformation*, 37, 56–64. <https://doi.org/10.1016/j.jag.2014.09.002>
- Rokni, K., Ahmad, A., Solaimani, K., & Hazini, S. (2015). A new approach for surface water change detection: Integration of pixel level image fusion and image classification techniques. *International Journal of Applied Earth Observation and Geoinformation*, 34, 226–234. <https://doi.org/10.1016/j.jag.2014.08.014>
- Salih, A. (2018). Classification and mapping of land cover types and attributes in Al-Ahsaa Oasis, Eastern Region, Saudi Arabia Using Landsat-7 Data. *Journal of Remote Sensing & GIS*, 7, 228. <https://doi.org/10.4172/2469-4134.1000228>
- Singh, A. (1989). Digital change detection techniques using remotely sensed data. *International Journal of Remote Sensing*, 10(6), 989–1000. <https://doi.org/10.1080/01431168908903939>
- Solberg, A., Taxt, T., & Jain, A. K. (1996). A Markov random field model for classification of multisource satellite imagery. *IEEE Transactions on Geoscience and Remote Sensing*, 34(1), 100–113.
- Tolpekin, V. A., & Stein, A. (2009). Quantification of the effects of land-cover-class spectral separability on the accuracy of Markov-random-field-based superresolution mapping. *IEEE Transactions on Geoscience and Remote Sensing*, 47(9), 3283–3297. <https://doi.org/10.1109/TGRS.2009.2019126>
- UNITED STATES GEOLOGICAL SURVEY (2022). Landsat Satellite Missions. Available at: <https://earthexplorer.usgs.gov/>
- Wang, J., Yong Gea, Y., Heuvelink, G., Zhoua, C., & Brusd, D. (2012). Effect of the sampling design of ground control points on the geometric. *International Journal of Applied Earth Observation and Geoinformation*, 18, 91–100. <https://doi.org/10.1016/j.jag.2012.01.001>
- Wu, C., Du, B., Cui, X., & Zhang, L. (2017). A post-classification change detection method based on iterative slow feature analysis and Bayesian soft fusion. *Remote Sensing of Environment*, 199, 241–255. <https://doi.org/10.1016/j.rse.2017.07.009>
- Xu, T., Weng, B., Yan, D., Wang, K., Li, X., Bi, W., Li, M., Cheng, X., & Liu, Y. (2019). Wetlands of International Importance: Status, threats, and future protection. *International Journal of Environmental Research and Public Health*, 16, 1818. <https://doi.org/10.3390/ijerph16101818>
- Youssef, A. M., Al-Fredan, M. A., Adel, A., & Fathi, A. A. (2009). Floristic composition of Lake Al-Asfar, Alahsa, Saudi Arabia. *International Journal of Botany*, 5, 116–125. <https://doi.org/10.3923/ijb.2009.116.125>
- Zheng, Ch., Pan, X., Chen, X., Yang, X., Xin, X., & Su, L. (2019). An object-based markov random field model with anisotropic penalty for semantic segmentation of high spatial resolution remote sensing imagery. *Remote Sensing*, 11(23), 2878. <https://doi.org/10.3390/rs11232878>
- Zheng, C., & Yao, H. (2019). Segmentation for remote-sensing imagery using the object-based Gaussian-Markov random field model with region coefficients. *International Journal of Remote Sensing*, 40, 4441–4472. <https://doi.org/10.1080/01431161.2018.1563841>

Publisher's Note Springer Nature remains neutral with regard to jurisdictional claims in published maps and institutional affiliations.

Springer Nature or its licensor (e.g. a society or other partner) holds exclusive rights to this article under a publishing agreement with the author(s) or other rightsholder(s); author self-archiving of the accepted manuscript version of this article is solely governed by the terms of such publishing agreement and applicable law.